Intensity-Modulated Scanning Kelvin Probe Microscopy for Probing Recombination in Organic Photovoltaics

Guozheng Shao,[†,∥] Micah S. Glaz,[†,∥] Fei Ma,[†,‡] Huanxin Ju,[†,§] and David S. Ginger*[,†]

[†]Department of Chemistry, University of Washington, Seattle, Washington 98195-1700, United States, [‡]School of Physical Science and Technology, Lanzhou University, Lanzhou, Gansu 730000, People's Republic of China, and [§]National Synchrotron Radiation Laboratory, University of Science and Technology of China, Hefei, Anhui 230029, People's Republic of China. [∥]These authors (G.S. and M.S.G.) contributed equally.

ABSTRACT We study surface photovoltage decays on sub-millisecond time scales in organic solar cells using intensity-modulated scanning Kelvin probe microscopy (SKPM). Using polymer/fullerene (poly[*N*-9″-heptadecanyl-2,7-carbazole-*alt*-5,5-(4′,7′-di-2-thienyl-2′,1′,3′-benzothiadiazole)]/[6,6]-phenyl C_{71}-butyric acid methyl ester, PCDTBT/$PC_{71}BM$) bulk heterojunction devices as a test case, we show that the decay lifetimes measured by SKPM depend on the intensity of the background illumination. We propose that this intensity dependence is related to the well-known carrier-density-dependent recombination kinetics in organic bulk heterojunction materials. We perform transient photovoltage (TPV) and charge extraction (CE) measurements on the PCDTBT/$PC_{71}BM$ blends to extract the carrier-density dependence of the recombination lifetime in our samples, and we find that the device TPV and CE data are in good agreement with the intensity and frequency dependence observed *via* SKPM. Finally, we demonstrate the capability of intensity-modulated SKPM to probe local recombination rates due to buried interfaces in organic photovoltaics (OPVs). We measure the differences in photovoltage decay lifetimes over regions of an OPV cell fabricated on an indium tin oxide electrode patterned with two different phosphonic acid monolayers known to affect carrier lifetime.

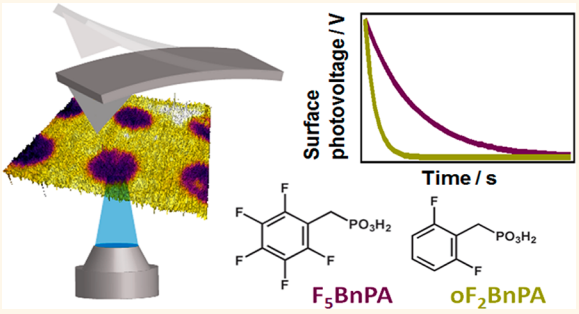

KEYWORDS: scanning Kelvin probe microscopy · organic photovoltaic · recombination kinetics · surface modification

The performance of organic photovoltaics (OPVs) has improved rapidly over the past decade and now exceeds 11%.[1] However, despite these impressive gains, the performance of even a 10% efficient OPV still falls short of the theoretical efficiencies of 20+% that have been predicted by many authors.[2,3] In order to understand this gap, there have been extensive studies on the sources of recombination losses[4−9] that can reduce the short-circuit current (J_{SC}), fill factor (FF), and open-circuit voltage (V_{OC}) of OPVs.

Work on interlayer materials ranging from transition metal oxides[10−12] to self-assembled monolayers[6,13−17] has shown that interface properties can play an important role in controlling FF and V_{OC}, in particular. Similarly, control of molecular ordering and compositional gradients at buried interfaces has been proposed as key criteria in the demonstration of OPVs with FFs of 80%.[18] However, understanding the role that buried interfaces play in OPV performance remains complicated by the fact that these interfaces are often heterogeneous.[19−22]

Exploring the role of heterogeneity in recombination remains difficult because some of the most common approaches to studying recombination such as charge extraction by linearly increasing voltage,[23] JV modeling,[24] intensity-dependent photocurrent,[25] time-resolved microwave conductivity,[26] photoinduced absorption at different pump fluences,[8] intensity-modulated photocurrent and photovoltage,[27,28] transient photocurrent,[29] and TPV[9,30,31] average sample properties over macroscopic areas, making them unsuitable for directly assessing the role that local heterogeneity plays

* Address correspondence to ginger@chem.washington.edu.

Received for review August 15, 2014 and accepted September 10, 2014.

Published online September 10, 2014
10.1021/nn5045867

in OPV devices. In the context of OPVs, methods such as confocal optical microscopy,[32−35] scanning near-field optical microscopy,[36−38] and an array of electrical scanning probe methods such as conductive and photoconductive atomic force microscopy (AFM)[19,39−42] and electrostatic force microscopy (EFM)[43−50] have been used to explore the connections between structural heterogeneity and function in OPVs—though to date most of these methods have not been used to measure local carrier recombination rates.

Notably, however, the influence of local structural heterogeneity is not limited to OPVs. Indeed, the influence of grain boundaries on recombination kinetics is a key question facing many thin-film inorganic photovoltaic technologies ranging from copper zinc tin sulfide[51,52] to the new hybrid perovskites.[53] To address this question, Takihara *et al.* have used scanning Kelvin probe microscopy (SKPM) with modulated photoexcitation to measure the photovoltage decay and thus extract local carrier lifetimes and recombination rates as a function of position near grain boundaries in materials such as polycrystalline Si.[54]

Here, we modify this photoassisted intensity-modulated SKPM method to the study of carrier recombination in OPVs. We use the model polymer/fullerene blend of poly[*N*-9″-heptadecanyl-2,7-carbazole-*alt*-5,5-(4′,7′-di-2-thienyl-2′,1′,3′-benzothiadiazole)]/[6,6]-phenyl C_{71}-butyric acid methyl ester (PCDTBT/$PC_{71}BM$). Importantly, we study the dependence of the signal on the modulated light intensity, as well as the effect of using a background bias light source. We demonstrate that these parameters have a significant influence on the measured lifetimes due to the strong dependence of transport and recombination kinetics on carrier density in OPVs. Importantly, we show that the kinetics measured by SKPM are consistent with those measured by TPV in a completed device. Finally, we demonstrate that intensity-modulated SKPM can be used to distinguish variations in carrier dynamics due to chemical heterogeneity at a buried interface.

RESULTS AND DISCUSSION

We studied model bulk heterojunction films and devices in standard geometries consisting of ITO/PEDOT:PSS/PCDTBT:$PC_{71}BM$/Al, with active layer thicknesses of ∼80 nm. Using the processing conditions described in the Experimental Section, we obtained typical power conversion efficiencies (PCEs) of 4.3%, with V_{OC} = 0.86 V, J_{SC} = 8.1 mA/cm^2, and FF = 0.62 (Figure 1A) under simulated AM 1.5 illumination. Although the V_{OC} and PCE are slightly below the best reported values for PCDTBT films,[55,56] these numbers are consistent with the range of literature values for this material that are commonly reported.[29] Figure 1B shows a typical intermittent contact AFM topography scan of the corresponding film, showing fairly smooth films, with rms roughnesses of 0.5 nm. This fine-scale surface morphology is well-suited to the current experiments, as here we are primarily interested in studying the general process of measuring photovoltage decays *via* SKPM than resolving specific structures.

As shown in Figure 1C, we measured surface photovoltages with the SKPM tip on the top surface of the PCDTBT/$PC_{71}BM$ blends in areas without metal top contacts (we measured V_{OC} on the metalized pixels, in conventional fashion). Figure 2 plots both the

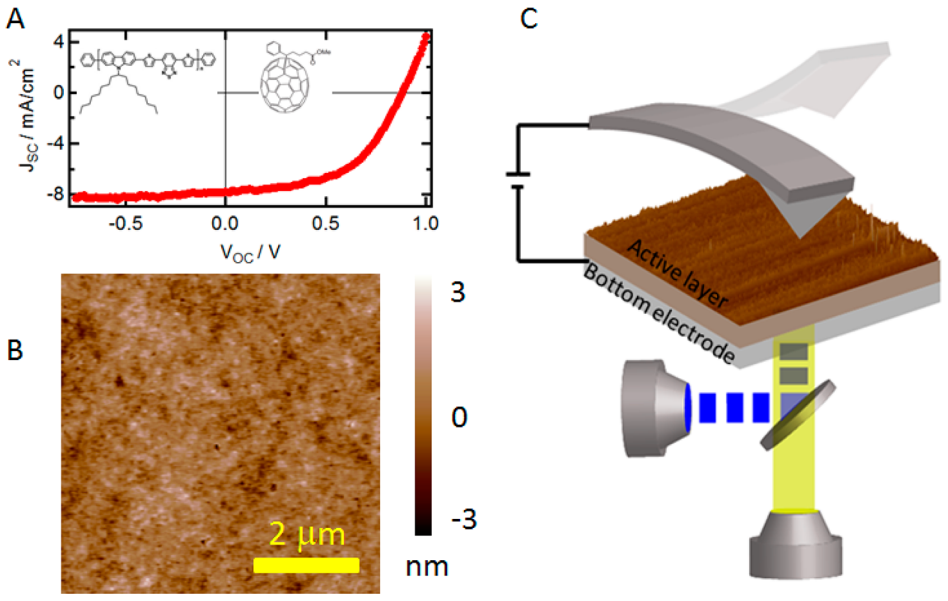

Figure 1. (A) *J*−*V* curve of a typical PCDTBT:$PC_{71}BM$ device used in this study. (B) Intermittent contact mode AFM topography of a typical PCDTBT:$PC_{71}BM$ blend as cast on PEDOT:PSS on ITO. (C) Experimental scheme showing the illumination geometry with white background illumination and modulated blue illumination coming under the AFM tip through an inverted microscope objective lens.

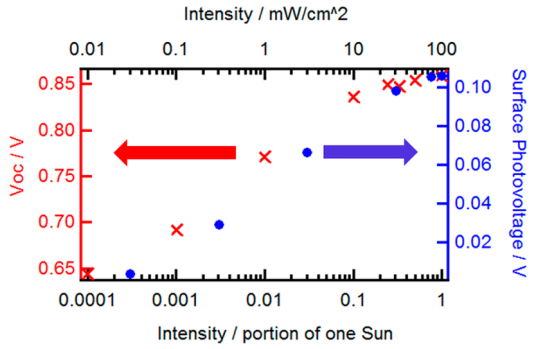

Figure 2. V_{OC} measured from a device (red crosses) and surface potential measured from SKPM (blue dots) at different light intensities.

surface photovoltage (blue) and V_{OC} (red) as a function of light intensity. Upon illumination, the PCDTBT/$PC_{71}BM$ films develop a negative surface photovoltage. This negative photovoltage indicates the accumulation of excess hole carriers at the film surface in the steady state, in good agreement with the detailed SKPM and modeling studies performed by Kemerink and coworkers on MDMO-PPV/$PC_{61}BM$ blends.[46] The data in Figure 2 show that both the V_{OC} (measured in a device configuration) and surface photovoltage (measured *via* SKPM without a top contact) show a similar functional form. This result is consistent with the expectation that both V_{OC}[57] and surface photovoltage (SPV)[58] typically show a logarithmic dependence on light intensity. At higher intensities, we observe that both V_{OC} and surface photovoltage saturate, as is consistent with expectations from previous experiments on a range of materials.[59,60] Indeed, Figure 2 shows that the saturation occurs at similar light intensity for both V_{OC} and SPV, despite the differences in total potential.

When the illumination is removed, both the V_{OC} of the device and SPV in the SKPM geometry decay with time (see below). The decay of the V_{OC} in a device geometry forms the basis for the TPV method of measuring carrier recombination rates.[6,9] Similarly, Takihara *et al.* have previously used surface photovoltage decays as a way to measure *local* carrier lifetimes in the frequency domain in microstructured inorganic PVs using SKPM to measure the resulting time-averaged voltage while the intensity of the excitation light source is modulated at varying frequency.[54] In organic bulk heterojunction films, Kemerink and coworkers have noted that the SPV decay exhibits both a slow (~minutes to hours) component associated with the filling and emptying of deep traps and a fast (~milliseconds or faster) component associated with the recombination of excess free carriers.[46] In our experiments with PCDTBT, we noticed minimal slow decay, with most of the photovoltage dissipating on time scales of ~milliseconds. To our knowledge, this fast recombination of the excess carrier population

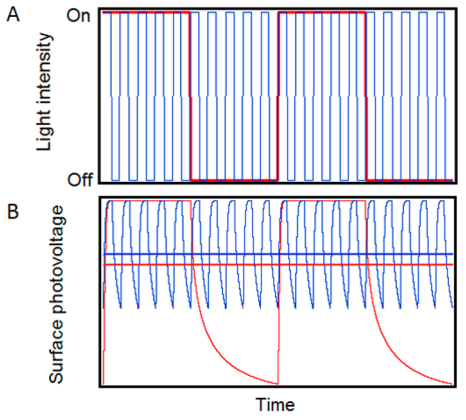

Figure 3. Schematics of the principle of intensity-modulated SKPM. (A) Light modulating periods of the LED, with the red trace being the modulation with a low frequency and blue trace being the modulation with a high frequency. (B) Oscillations of the sample surface potential as a result of the LED modulation. The horizontal lines are the time-averaged values recorded by the instrument.

in OPVs has so far not been resolvable in time using scanning probe microscopy.

In order to study this fast photovoltage decay component in more detail, we adopted the experimental geometry of Takihara *et al.* (Figure 1C), with the key critical addition of a DC white light bias. Conceptually, the experiment in Figure 1C is straightforward: a probe light source is rapidly switched on and off while an SKPM tip is used to measure the local time-averaged surface potential. When the probe light is on, excess carrier accumulation leads to a change in surface potential compared to the dark state. When the probe light is turned off, this excess population decays with a functional form that depends on the physics of the process(es) governing the decay of that excess population. Since SKPM is inherently a slow technique, the SKPM acts as a low-pass filter giving a time-averaged photovoltage. Figure 3 depicts how the frequency dependence of the time-averaged SKPM signal can, in principle, be used to extract local variations in the lifetime of the excess photogenerated carriers. Importantly, our addition of a white light bias allows us to measure the change in decay rate as we use the DC light bias to control the background carrier concentration in the film.

As is clear from Figure 3, the exact functional form of the SKPM magnitude *versus* frequency data will depend on the kinetics of the underlying recombination process. However, in general, one expects the measured SKPM signal to saturate at a maximum value at high frequency (when the light is being modulated faster than the system can respond) and a minimum value at low frequency (at which point the measured SKPM signal is just the time average of the equilibrated surface potentials measured in the "light-off" and the "light-on" states).[54] The midpoint between these two regimes will happen near the dominant characteristic lifetime of the system.

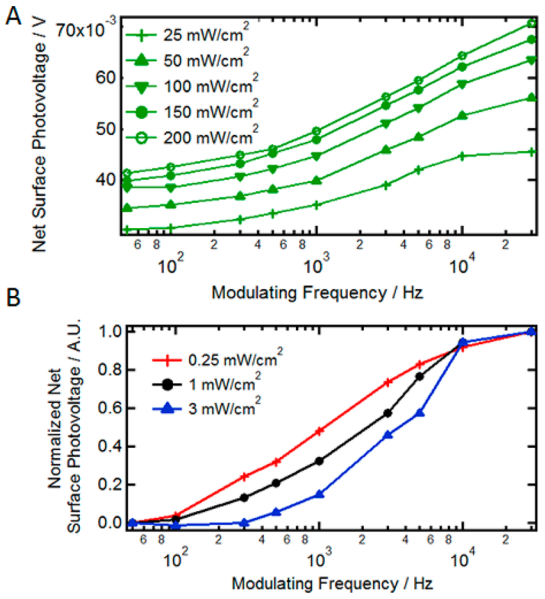

Figure 4. (A) Time-averaged surface photovoltage plotted against modulation frequency with varying peak modulation intensity (470 nm probe LED as the excitation source) with a fixed white light background intensity of 1 mW/cm^2. Each curve was done with a different probing intensity as indicated in the figure. Each point in the figure is a time-averaged surface photovoltage value over a 30 s period. Lines are guides for the eye. (B) Time-averaged surface photovoltage plotted against modulation frequency with constant peak modulated light intensity (25 mW/cm^2) and varying background illumination intensity of 0.25, 1, and 3 mW/cm^2. Lines are guides for the eye.

Figure 4 shows experimental intensity-modulated SKPM data taken on PCDTBT/$PC_{71}BM$ films plotted as the surface photovoltage measured *versus* the probing light modulation frequency. Figure 4A shows the effect of varying the peak probe light intensity from 25 to 200 mW/cm^2 (~25 to 200% 1.5 AM one sun intensity) while keeping the white bias LED at a constant intensity of 1 mW/cm^2, whereas Figure 4B shows the effect of varying the background white light intensity from 0.25 to 3 mW/cm^2 while keeping the peak intensity of the modulated 470 nm LED fixed at 25 mW/cm^2. As expected, Figure 4A shows that as the peak intensity of the modulated probe light is increased, the average photovoltage increases for all modulation frequencies. This result is easy to understand: as already shown in Figure 2, the surface photovoltage increases with light intensity. Thus, increasing the maximum intensity of the modulated light increases the time-averaged photovoltage as measured by SKPM at all modulation frequencies.

Figure 4B shows how the frequency dependence of the surface photovoltage changes as a function of varying constant background illumination intensity. The general shape of the curves is as expected—the average photovoltage tends to increase with modulation frequency, before leveling off at high frequency.[54] Importantly, however, the midpoints of the frequency dependence curves shift toward higher frequencies with increasing background light intensity, as would be expected if the photovoltage lifetime was decreasing at higher light intensities. While an intensity-dependent carrier lifetime has not previously been considered when analyzing intensity-modulated SKPM data on inorganic semiconductors,[54] carrier-density-dependent lifetimes have been widely reported in the OPV literature,[6,9,61,62] including for PCDTBT/$PC_{71}BM$ blends.[62] We therefore propose that the carrier-density-dependent lifetime observed in OPVs is responsible for the decrease in lifetime we measure with the intensity-modulated SKPM as the background light intensity is increased. The intensity-modulated SKPM data shown are for a single point on each sample. Although there are some spatial variations in the quantitative values, we confirmed that the overall trends in intensity and frequency that we focus on here are representative of the PCDTBT:$PC_{71}BM$ samples in general (see Supporting Information Figure S9 for data taken at multiple locations on different samples). We have tested the consistency of these results across different points and different samples prepared identically. The general trends shown in Figure 4B held for all points and samples (see Supporting Information Figure S9). While we expect that there is likely some variation due to local film morphology effects, these variations are not large enough to interfere with the general properties such as the frequency dependence of the photovoltage and the intensity dependence of the carrier lifetime that we are concerned with herein.

To investigate the relationship between the intensity-dependent surface photovoltage lifetime measured in our SKPM experiments and the recombination lifetimes more typically measured on completed organic photovoltaic devices, we performed TPV[6,9] and charge extraction (CE)[6,9] on the same PCDTBT/$PC_{71}BM$ films used in the SKPM experiments as a function of background light intensity using methods previously described (see Supporting Information).[6] Briefly, TPV measures the pseudo-first-order carrier recombination rate by measuring the decay of a small voltage transient induced in a device by a weak transient perturbation light pulse while the carrier density in the cell is held fixed using a continuous white light bias and a high impedance load. CE measures the carrier density in a device by shunting an illuminated device through a small series resistor at the same time the illumination is extinguished and then measures the resulting total integrated charge.

Figure 5 shows the TPV data obtained on PCTDTB/$PC_{71}BM$ films. Figure 5 plots $\tau_{\Delta n}$, the small perturbation (pseudo-first-order) voltage decay lifetime, as a function of V_{OC} (also see Supporting Information Figures S3−S5 for carrier-density-dependent lifetime). It is clear that $\tau_{\Delta n}$ is strongly dependent on light intensity/carrier density, as has been reported previously for PCDTBT/fullerene blends,[62] as well as many other polymer bulk heterojunction materials.[6,9,61,62] Consistent with previous

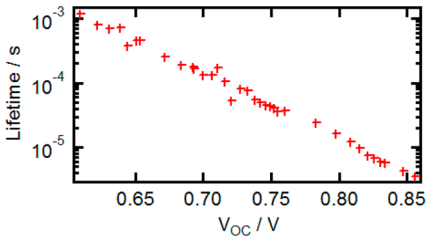

Figure 5. Lifetime of charge carriers at different V_{OC} by varying the illumination intensity under the TPV setup.

reports, the lifetime decreases rapidly with increasing carrier density, exhibiting an apparent recombination order >2. Recombination order is the order of annihilation reaction between electrons and holes,[4,9] and reaction orders >2 have been commonly attributed to carrier-dependent mobility in organic semiconductors.[9,63]

The TPV data in Figure 5 are qualitatively consistent with the SKPM data in Figure 4. Both experiments suggest that the recovery kinetics are faster at higher carrier density. Unlike with TPV or intensity-modulated photocurrent techniques, signal-to-noise limitations make it difficult for us to conduct SKPM measurements in the small perturbation limit. As a result, the modulated light intensity causes changes in the carrier concentration that can be comparable to, or even larger than, those induced by the bias light. In this case, the background illumination, rather than holding the carrier concentration effectively constant as in a TPV experiment, serves here to prevent the carrier concentration from dropping below a fixed level. We emphasize that intensity-modulated SKPM and TPV therefore probe different characteristic lifetimes, and it is only through modeling (as shown below) that we can compare them directly. We next showed that these data are quantitatively consistent by using the experimental carrier recombination kinetics as determined by TPV to simulate both the frequency and background intensity dependence of the intensity-modulated SKPM data. For the simulation, we performed a numerical integration of the carrier kinetics in the time domain using the known light intensity and film absorbance values to vary the generation rate and the TPV-derived τ *versus* n data to determine the instantaneous carrier recombination rate at each integration step (see Supporting Information Figures S3 and S4 and eqs S1 and S2 for details). These simulations produced voltage *versus* time plots. Since the SKPM measures the time-averaged voltage, we then computed the time average of the simulated voltage at each intensity and modulation frequency.

Figure 6 plots the results of the intensity-modulated SKPM data as simulated using the experimental TPV data as input. The simulation reproduces both key qualitative trends, as well as the quantitative values of the experimental data in Figure 4. Notably, as the optical modulation frequency is increased, the

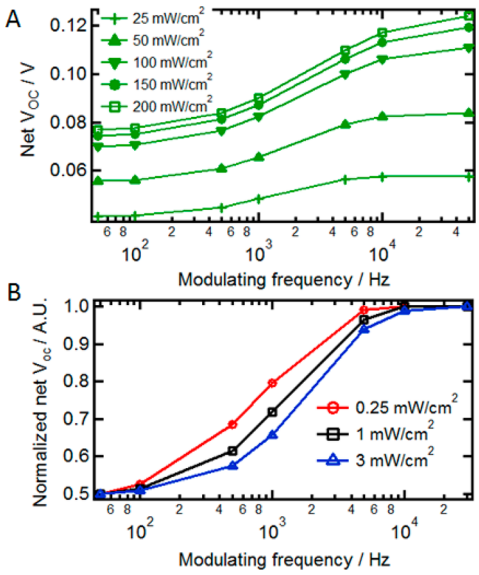

Figure 6. Simulated V_{OC} decay under modulating frequency. Decay of V_{OC} *vs* time is described by Supporting Information eq S2. Different time period was used to simulate V_{OC} decay. (A) Fixed 1 mW/cm^2 background illumination and varying probing illumination as indicated in the figure. (B) Fixed probing intensity of 25 mW/cm^2 with varying background illumination as indicated. Net V_{OC} means the increase of V_{OC} due to the probing illumination. Each point in the figure is a time-averaged V_{OC} value. This figure is plotted in the frequency domain for more direct comparison with SKPM data.

time-averaged surface photovoltage increases with the same S-shaped curve, as shown in Figure 2. More importantly, as the background illumination intensity is increased, the midpoint frequency at which the photovoltage reaches half of the saturation value shifts to higher frequencies/faster lifetimes. Remarkably, the midpoint frequency values (reflecting a weighted average of the lifetime distribution) simulated from the TPV data agree within better than a factor of 2 with the experimental values. Given the experimental limitations of the TPV and CE data, we conclude that the data are remarkably consistent with the TPV decays and the SKPM decays sharing the same underlying kinetics.

Previously, we have shown that the recombination lifetimes measured in TPV can be strongly influenced by the surface chemistry at the hole-extracting contact.[6] Given that the SKPM experiment seems to be probing the same underlying kinetics as the TPV experiment, we next asked if it would be possible to use intensity-modulated SKPM to measure spatial variations in carrier lifetimes due to chemical heterogeneity at a buried active layer/hole-extraction layer interface. Such studies are useful because the hole-extraction layer can be very heterogeneous,[19,20,22] and understanding how recombination is affected at the buried interface could lead to better-engineered interfaces.

In order to demonstrate this possibility of using SKPM to probe recombination at the buried contacts in OPVs, we used microcontact printing to generate phosphonic acid patterns on ITO electrodes prior to

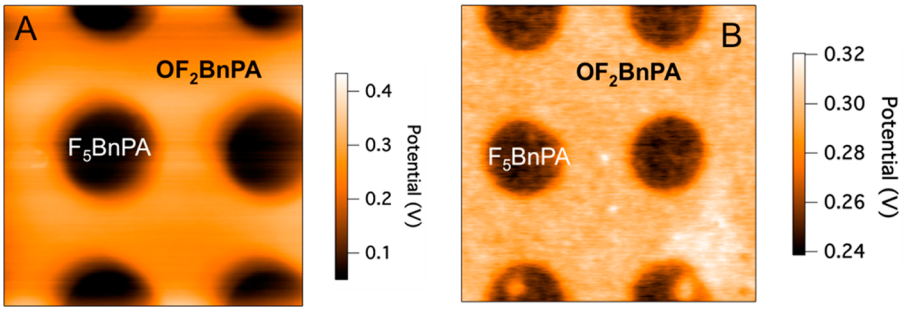

Figure 7. (A) Surface potential map of ITO modified with 2,6-difluorobenzylphosphonic acid (oF_2BnPA, orange) and pentafluorobenzylphosphonic acid (F_5BnPA, black). (B) Surface potential of PCDTBT:$PC_{71}BM$ film spin-coated over the modified ITO substrate pattern under illumination.

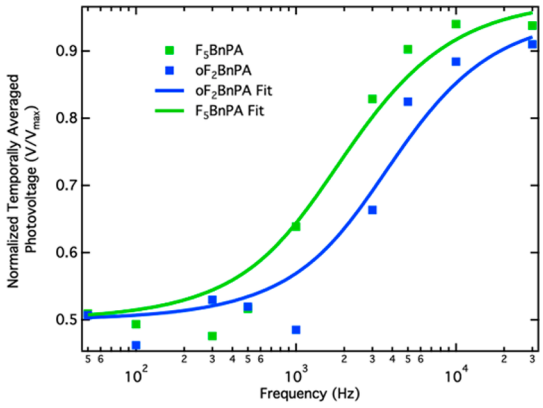

Figure 8. Time-averaged surface photovoltage measured at different LED modulating frequency with intensity-modulated SKPM measurement. Sample is a PCDTBT:$PC_{71}BM$ layer over an ITO substrate patterned with oF_2BnPA and F_5BnPA. The blue and green dots are experimental data for areas over oF_2BnPA and F_5BnPA, respectively. Lines are fits of stretched exponential in the frequency domain with characteristic lifetimes of τ = 1.1 ms (F_5BnPA) and τ = 0.51 ms (oF_2BnPA) and stretching exponent β = 1.08 (F_5BnPA) and β = 1.17 (oF_2BnPA).

depositing the active semiconductor layer.[17] Figure 7A shows an SKPM image of the resulting patterned ITO electrode. The ~0.3 eV work function contrast is due to the difference in surface dipoles between the two phosphonic acids.[17] Figure 7B shows the surface potential contrast with the PCDTBT/$PC_{71}BM$ blend on top of the ITO and under 12.5 mW/cm^2 of illumination. Due to band banding in the overlying semiconductor, the surface potential contrast is attenuated (contrast ~50 mV) from that of the bare electrode, but the pattern is still visible in the SKPM image. This residual SKPM contrast allows us to locate the SKPM tip above regions of known surface chemistry and acquire spatially resolved, intensity-modulated SKPM data.

Figure 8 shows the local surface photovoltage measured with SKPM as a function of modulation frequency over regions of the PCDTBT/$PC_{71}BM$ film that have either pentafluorobenzylphosphonic acid (F_5BnPA, larger work function) or 2,6-difluorobenzylphosphonic acid (oF_2BnPA, smaller work function) underneath. The curve taken over the oF_2BnPA region is shifted systematically to higher frequencies, indicating that the photovoltage decay is faster over the oF_2BnPA-patterned region as compared to that of the F_5BnPA. Figure 8 also shows stretched exponential fits to the experimental data (see Supporting Information eq S4 for fitting details). Using these fits, we extract a characteristic carrier lifetime that is ~2 times faster for oF_2BnPA than for F_5BnPA at a given light intensity. This result is in good agreement with TPV data taken on devices made with phosphonic-acid-treated electrodes, where oF_2BnPA-treated electrodes exhibited consistently faster TPV lifetimes as compared to F_5BnPA-treated electrodes.[6] We thus conclude that intensity-modulated SKPM can be applied to measure variations in carrier lifetimes due to heterogeneity in the buried electrode surface chemistry.

CONCLUSIONS

In summary, we have studied intensity-modulated SKPM on model polymer solar cells consisting of PCDTBT/$PC_{71}BM$ bulk heterojunctions. We find that the ~millisecond scale surface photovoltage decays measured *via* SKPM exhibit intensity-dependent recombination kinetics, in quantitative agreement with the carrier recombination kinetics measured in bulk devices by TPV. Furthermore, we have shown that we can use intensity-modulated SKPM to probe variations in carrier kinetics due to heterogeneity in the buried surface chemistry. Broadly, these results not only support the contention that carrier kinetics in polymer solar cells are sensitive to surface chemistry[6,14,18] but also suggest that any heterogeneity in surface chemistry could lead to potentially detrimental effects on recombination lifetimes at the electrode interfaces.

EXPERIMENTAL SECTION

Device Fabrication. Bulk heterojunction solar cells made from PCDTBT (poly[*N*-11″-henicosanyl-2,7-carbazole-*alt*-5,5-(4′,7′-di-2-thienyl-2′,1′,3′-benzothiadiazole)]:$PC_{71}BM$ (phenyl-C_{71}-butyric acid methyl ester) were used in this study. PCDTBT was purchased from St-Jean Photochemical Inc. and $PC_{71}CM$ from

Nano-C. PCDTBT and $PC_{71}BM$ were blended in a 1:4 ratio in a dichlorobenze/trichlorobenzene mixed solution in (1:2 weight ratio of solvents) to achieve a combined PCDTBT + $PC_{71}BM$ concentration of 30 mg/mL. This final solution was spin-coated on top of a 30 nm thick PEDOT:PSS layer on an ITO substrate to achieve an 80 nm active layer. A 40 nm Al top electrode was evaporated inside a thermal evaporator with a custom-made evaporation mask exposing only part of the surface to coverage by the top metal electrode (for device characterization and TPV experiments as will be discussed later) and leaving part of the active layer film exposed for SKPM experiments.

Patterning ITO with Phosphonic Acids. 2,6-Difluorobenzylphosphonic acid (oF_2BnPA) and pentafluorobenzylphosphonic acid (F_5BnPA) were used to pattern work function variations on the substrate.[17] The ITO substrates were first sonicated in acetone for 15 min and blown dry with nitrogen. They were then sonicated in isopropyl alcohol for 15 min and blown dry with nitrogen. Afterward, the ITO was placed within a plasma cleaner (Harrick plasma cleaner PCD32G) for plasma cleaning for 5 min with air. Immediately after removal from the plasma cleaner, the substrate was micro-contact-printed with a PDMS stamp using a 10 mM ethanolic solution of F_5BnPA as the ink and then annealed at 140 °C for 5 min. The substrate was then rinsed and soaked in a 10 mM ethanolic solution of oF_2BnPA overnight, then rinsed with ethanol and annealed at 140 °C for 5 min a second time. The substrates were then sonicated in 5% triethylamine/95% EtOH solution for 30 min. The active layer of PCDTBT:$PC_{71}BM$ was then spin-coated on top the phosphonic-acid-covered ITO substrates.

AFM. SKPM measurements were carried out on an MFP-3D-BIO-based (Asylum Research) AFM with custom modifications using 300 kHz Pt-coated cantilevers (BudgetSensor ElectriTap300). SKPM was carried out in a flow cell with active nitrogen flow, at a lift height of 50 nm. The flow cell used here has a ~1.5−2.5 mL fluid volume after engaging the tip. The SKPM setup is displayed in Figure 1C. The 455 nm LED was purchased from LED Engin (product numbers LZ1-00DB00). The incident illumination power was calibrated using a Si diode.

TPV and CE Measurements. TPV and CE measurements were performed on a home-built system as described elsewhere.[6] Briefly, background illumination was provided by a white LED (Bridgelux BXRA-56C9000-J) which was driven by a TTI instrument power supply (CPX400SA) and controlled through a custom LabVIEW program. A 447.5 nm LED (Luxeon Star LXML-PR01-0425) was driven (electrical pulse of 2 Hz, 4 μs width, 20 ns edge) by a home-built LED driver circuit and waveform generator (Agilent 33210A). Samples were mounted in a home-built vacuum chamber and tested under active vacuum (typically between 5 and 15 mTorr). The device was held at open circuit through a buffer with a 500 GΩ effective input impedance, and the resulting transient voltage across the cell was measured by an oscilloscope (Textronix TDS 2024B). CE measurements employed a home-built circuit that allowed the device to be switched from open circuit to short circuit. The device's extracted current was shunted through a 510 Ω resistor. The corresponding voltage decay transient was again measured by the oscilloscope. After data collection, the voltage transient was converted to a current transient using Ohm's Law and used to determine a current volume. Charge carrier density (n) was calculated by integrating the area underneath the transient and dividing by the charge on an electron.

Conflict of Interest: The authors declare no competing financial interest.

Acknowledgment. We thank the Marder group at GaTech for supplying the phosphonic acids used in this study. This paper is based primarily on research that was supported as part of the Center for Interface Science: Solar Electric Materials (CISSEM), an Energy Frontier Research Center funded by the U.S. Department of Energy (DOE), Office of Science, Basic Energy Sciences (BES), under Award Number DE-SC0001084.

Supporting Information Available: Diagrams showing TPV and CE setups, fittings of the TPV and CE data, numerical simulation procedures of V_{OC} decay, and fitting equation of stretched exponential. This material is available free of charge *via* the Internet at http://pubs.acs.org.

Note Added after ASAP Publication: After this paper was published ASAP on September 15, 2014, text was added to the Acknowledgment. The corrected version was reposted September 23, 2014.

REFERENCES AND NOTES

1. Green, M. A.; Emery, K.; Hishikawa, Y.; Warta, W.; Dunlop, E. D. Solar Cell Efficiency Tables (Version 43). *Prog. Photovoltaics* **2014**, *22*, 1–9.
2. Giebink, N. C.; Wiederrecht, G. P.; Wasielewski, M. R.; Forrest, S. R. Thermodynamic Efficiency Limit of Excitonic Solar Cells. *Phys. Rev. B* **2011**, *83*, 195326.
3. Koster, L. J. A.; Shaheen, S. E.; Hummelen, J. C. Pathways to a New Efficiency Regime for Organic Solar Cells. *Adv. Energy Mater.* **2012**, *2*, 1246–1253.
4. Deibel, C.; Baumann, A.; Dyakonov, V. Polaron Recombination in Pristine and Annealed Bulk Heterojunction Solar Cells. *Appl. Phys. Lett.* **2008**, *93*, 163303.
5. Mayer, A. C.; Toney, M. F.; Scully, S. R.; Rivnay, J.; Brabec, C. J.; Scharber, M.; Koppe, M.; Heeney, M.; McCulloch, I.; McGehee, M. D. Bimolecular Crystals of Fullerenes in Conjugated Polymers and the Implications of Molecular Mixing for Solar Cells. *Adv. Funct. Mater.* **2009**, *19*, 1173–1179.
6. Knesting, K. M.; Ju, H. X.; Schlenker, C. W.; Giordano, A. J.; Garcia, A.; Smith, O. L.; Olson, D. C.; Marder, S. R.; Ginger, D. S. ITO Interface Modifiers Can Improve V_{OC} in Polymer Solar Cells and Suppress Surface Recombination. *J. Phys. Chem. Lett.* **2013**, *4*, 4038–4044.
7. Schlenker, C. W.; Chen, K.-S.; Yip, H.-L.; Li, C.-Z.; Bradshaw, L. R.; Ochsenbein, S. T.; Ding, F.; Li, X. S.; Gamelin, D. R.; Jen, A. K. Y.; *et al.* Polymer Triplet Energy Levels Need Not Limit Photocurrent Collection in Organic Solar Cells. *J. Am. Chem. Soc.* **2012**, *134*, 19661–19668.
8. Rao, A.; Chow, P. C. Y.; Gelinas, S.; Schlenker, C. W.; Li, C. Z.; Yip, H. L.; Jen, A. K. Y.; Ginger, D. S.; Friend, R. H. The Role of Spin in the Kinetic Control of Recombination in Organic Photovoltaics. *Nature* **2013**, *500*, 435–439.
9. Shuttle, C. G.; O'Regan, B.; Ballantyne, A. M.; Nelson, J.; Bradley, D. D. C.; de Mello, J.; Durrant, J. R. Experimental Determination of the Rate Law for Charge Carrier Decay in a Polythiophene: Fullerene Solar Cell. *Appl. Phys. Lett.* **2008**, *92*, 093311-1–093311-3.
10. Irwin, M. D.; Buchholz, B.; Hains, A. W.; Chang, R. P. H.; Marks, T. J. p-Type Semiconducting Nickel Oxide as an Efficiency-Enhancing Anode Interfacial Layer in Polymer Bulk-Heterojunction Solar Cells. *Proc. Natl. Acad. Sci. U.S.A.* **2008**, *105*, 2783–2787.
11. Steirer, K. X.; Ndione, P. F.; Widjonarko, N. E.; Lloyd, M. T.; Meyer, J.; Ratcliff, E. L.; Kahn, A.; Armstrong, N. R.; Curtis, C. J.; Ginley, D. S.; *et al.* Enhanced Efficiency in Plastic Solar Cells *via* Energy Matched Solution Processed NiO_x Interlayers. *Adv. Energy Mater.* **2011**, *1*, 813–820.
12. Chen, S.; Manders, J. R.; Tsang, S. W.; So, F. Metal Oxides for Interface Engineering in Polymer Solar Cells. *J. Mater. Chem.* **2012**, *22*, 24202–24212.
13. Sharma, A.; Hotchkiss, P. J.; Marder, S. R.; Kippelen, B. Tailoring the Work Function of Indium Tin Oxide Electrodes in Electrophosphorescent Organic Light-Emitting Diodes. *J. Appl. Phys.* **2009**, *105*, 084507-1–084507-5.
14. Ratcliff, E. L.; Garcia, A.; Paniagua, S. A.; Cowan, S. R.; Giordano, A. J.; Ginley, D. S.; Marder, S. R.; Berry, J. J.; Olson, D. C. Investigating the Influence of Interfacial Contact Properties on Open Circuit Voltages in Organic Photovoltaic Performance: Work Function *versus* Selectivity. *Adv. Energy Mater.* **2013**, *3*, 647–656.
15. Gliboff, M.; Sang, L. Z.; Knesting, K. M.; Schalnat, M. C.; Mudalige, A.; Ratcliff, E. L.; Li, H.; Sigdel, A. K.; Giordano, A. J.; Berry, J. J.; *et al.* Orientation of Phenylphosphonic Acid Self-Assembled Monolayers on a Transparent Conductive Oxide: A Combined NEXAFS, PM-IRRAS, and DFT Study. *Langmuir* **2013**, *29*, 2166–2174.
16. Gliboff, M.; Li, H.; Knesting, K. M.; Giordano, A. J.; Nordlund, D.; Seidler, G. T.; Bredas, J. L.; Marder, S. R.; Ginger, D. S. Competing Effects of Fluorination on the Orientation of

Aromatic and Aliphatic Phosphonic Acid Monolayers on Indium Tin Oxide. *J. Phys. Chem. C* **2013**, *117*, 15139–15147.
17. Knesting, K. M.; Hotchkiss, P. J.; MacLeod, B. A.; Marder, S. R.; Ginger, D. S. Spatially Modulating Interfacial Properties of Transparent Conductive Oxides: Patterning Work Function with Phosphonic Acid Self-Assembled Monolayers. *Adv. Mater.* **2012**, *24*, 642–646.
18. Guo, X. G.; Zhou, N. J.; Lou, S. J.; Smith, J.; Tice, D. B.; Hennek, J. W.; Ortiz, R. P.; Navarrete, J. T. L.; Li, S. Y.; Strzalka, J.; *et al.* Polymer Solar Cells with Enhanced Fill Factors. *Nat. Photonics* **2013**, *7*, 825–833.
19. Nardes, A. M.; Kemerink, M.; Janssen, R. A. J.; Bastiaansen, J. A. M.; Kiggen, N. M. M.; Langeveld, B. M. W.; van Breemen, A. J. J. M.; de Kok, M. M. Microscopic Understanding of the Anisotropic Conductivity of PEDOT:PSS Thin Films. *Adv. Mater.* **2007**, *19*, 1196–1200.
20. Pingree, L. S. C.; MacLeod, B. A.; Ginger, D. S. The Changing Face of PEDOT:PSS Films: Substrate, Bias, and Processing Effects on Vertical Charge Transport. *J. Phys. Chem. C* **2008**, *112*, 7922–7927.
21. Brumbach, M.; Veneman, P. A.; Marrikar, F. S.; Schulmeyer, T.; Simmonds, A.; Xia, W.; Lee, P.; Armstrong, N. R. Surface Composition and Electrical and Electrochemical Properties of Freshly Deposited and Acid-Etched Indium Tin Oxide Electrodes. *Langmuir* **2007**, *23*, 11089–11099.
22. MacDonald, G. A.; Veneman, R. A.; Placencia, D.; Armstrong, N. R. Electrical Property Heterogeneity at Transparent Conductive Oxide/Organic Semiconductor Interfaces: Mapping Contact Ohmicity Using Conducting-Tip Atomic Force Microscopy. *ACS Nano* **2012**, *6*, 9623–9636.
23. Mozer, A. J.; Sariciftci, N. S.; Lutsen, L.; Vanderzande, D.; Osterbacka, R.; Westerling, M.; Juska, G. Charge Transport and Recombination in Bulk Heterojunction Solar Cells Studied by the Photoinduced Charge Extraction in Linearly Increasing Voltage Technique. *Appl. Phys. Lett.* **2005**, *86*, 112104-1–112104-3.
24. Street, R. A.; Schoendorf, M.; Roy, A.; Lee, J. H. Interface State Recombination in Organic Solar Cells. *Phys. Rev. B* **2010**, *81*, 205307.
25. Dibb, G. F. A.; Kirchartz, T.; Credgington, D.; Durrant, J. R.; Nelson, J. Analysis of the Relationship between Linearity of Corrected Photocurrent and the Order of Recombination in Organic Solar Cells. *J. Phys. Chem. Lett.* **2011**, *2*, 2407–2411.
26. Reid, O. G.; Rumbles, G. Quantitative Transient Absorption Measurements of Polaron Yield and Absorption Coefficient in Neat Conjugated Polymers. *J. Phys. Chem. Lett.* **2013**, *4*, 2348–2355.
27. Byers, J. C.; Ballantyne, S.; Rodionov, K.; Mann, A.; Semenikhin, O. A. Mechanism of Recombination Losses in Bulk Heterojunction P3HT:PCBM Solar Cells Studied Using Intensity Modulated Photocurrent Spectroscopy. *ACS Appl. Mater. Interfaces* **2011**, *3*, 392–401.
28. Set, Y. T.; Heinemann, M. D.; Birgersson, E.; Luther, J. On the Origin of the Quadrant I Semicircle in Intensity-Modulated Photocurrent Spectra of P3HT:PCBM Bulk Heterojunction Solar Cells: Evidence of Degradation-Related Trap-Assisted Recombination. *J. Phys. Chem. C* **2013**, *117*, 7993–8000.
29. Li, Z.; McNeill, C. R. Transient Photocurrent Measurements of PCDTBT:PC(70)BM and PCPDTBT:PC(70)BM Solar Cells: Evidence for Charge Trapping in Efficient Polymer/Fullerene Blends. *J. Appl. Phys.* **2011**, *109*, 074513-1–074513-7.
30. Credgington, D.; Jamieson, F. C.; Walker, B.; Nguyen, T. Q.; Durrant, J. R. Quantification of Geminate and Non-geminate Recombination Losses within a Solution-Processed Small-Molecule Bulk Heterojunction Solar Cell. *Adv. Mater.* **2012**, *24*, 2135–2141.
31. Hamilton, R.; Shuttle, C. G.; O'Regan, B.; Hammant, T. C.; Nelson, J.; Durrant, J. R. Recombination in Annealed and Nonannealed Polythiophene/Fullerene Solar Cells: Transient Photovoltage Studies *versus* Numerical Modeling. *J. Phys. Chem. Lett.* **2010**, *1*, 1432–1436.
32. Boroumand, F. A.; Fry, P. W.; Lidzey, D. G. Nanoscale Conjugated-Polymer Light-Emitting Diodes. *Nano Lett.* **2005**, *5*, 67–71.
33. Wong, C. Y.; Penwell, S. B.; Cotts, B. L.; Noriega, R.; Wu, H.; Ginsberg, N. S. Revealing Exciton Dynamics in a Small-Molecule Organic Semiconducting Film with Subdomain Transient Absorption Microscopy. *J. Phys. Chem. C* **2013**, *117*, 22111–22122.
34. Gao, Y. Q.; Grey, J. K. Resonance Chemical Imaging of Polythiophene/Fullerene Photovoltaic Thin Films: Mapping Morphology-Dependent Aggregated and Unaggregated C═C Species. *J. Am. Chem. Soc.* **2009**, *131*, 9654–9662.
35. Lombardo, C. J.; Glaz, M. S.; Ooi, Z. E.; Vanden Bout, D. A.; Dodabalapur, A. Scanning Photocurrent Microscopy of Lateral Organic Bulk Heterojunctions. *Phys. Chem. Chem. Phys.* **2012**, *14*, 13199–13203.
36. McNeill, C. R.; Frohne, H.; Holdsworth, J. L.; Dastoor, P. C. Near-Field Scanning Photocurrent Measurements of Polyfluorene Blend Devices: Directly Correlating Morphology with Current Generation. *Nano Lett.* **2004**, *4*, 2503–2507.
37. Riehn, R.; Stevenson, R.; Richards, D.; Kang, D. J.; Blamire, M.; Downes, A.; Cacialli, F. Local Probing of Photocurrent and Photoluminescence in a Phase-Separated Conjugated-Polymer Blend by Means of Near-Field Excitation. *Adv. Funct. Mater.* **2006**, *16*, 469–476.
38. Summers, M. A.; Buratto, S. K.; Edman, L. Morphology and Environment-Dependent Fluorescence in Blends Containing a Phenylenevinylene-Conjugated Polymer. *Thin Solid Films* **2007**, *515*, 8412–8418.
39. Coffey, D. C.; Reid, O. G.; Rodovsky, D. B.; Bartholomew, G. P.; Ginger, D. S. Mapping Local Photocurrents in Polymer/Fullerene Solar Cells with Photoconductive Atomic Force Microscopy. *Nano Lett.* **2007**, *7*, 738–744.
40. Dante, M.; Peet, J.; Nguyen, T. Q. Nanoscale Charge Transport and Internal Structure of Bulk Heterojunction Conjugated Polymer/Fullerene Solar Cells by Scanning Probe Microscopy. *J. Phys. Chem. C* **2008**, *112*, 7241–7249.
41. Moerman, D.; Lazzaroni, R.; Douheret, O. Efficient Bulk Heterojunction Photovoltaic Cells with a Pre-organized Poly(3-hexylthiophene) Phase. *Appl. Phys. Lett.* **2011**, *99*, 093303-1–093303-3.
42. Sengupta, E.; Domanski, A. L.; Weber, S. A. L.; Untch, M. B.; Butt, H. J.; Sauermann, T.; Egelhaaf, H. J.; Berger, R. Photo-induced Degradation Studies of Organic Solar Cell Materials Using Kelvin Probe Force and Conductive Scanning Force Microscopy. *J. Phys. Chem. C* **2011**, *115*, 19994–20001.
43. Coffey, D. C.; Ginger, D. S. Time-Resolved Electrostatic Force Microscopy of Polymer Solar Cells. *Nat. Mater.* **2006**, *5*, 735–740.
44. Shao, G. Z.; Rayermann, G. E.; Smith, E. M.; Ginger, D. S. Morphology-Dependent Trap Formation in Bulk Heterojunction Photodiodes. *J. Phys. Chem. B* **2013**, *117*, 4654–4660.
45. Liscio, A.; De Luca, G.; Nolde, F.; Palermo, V.; Muellen, K.; Samori, P. Photovoltaic Charge Generation Visualized at the Nanoscale: A Proof of Principle. *J. Am. Chem. Soc.* **2008**, *130*, 780–781.
46. Maturova, K.; Kemerink, M.; Wienk, M. M.; Charrier, D. S. H.; Janssen, R. A. J. Scanning Kelvin Probe Microscopy on Bulk Heterojunction Polymer Blends. *Adv. Funct. Mater.* **2009**, *19*, 1379–1386.
47. Luria, J. L.; Schwarz, K. A.; Jaquith, M. J.; Hennig, R. G.; Marohn, J. A. Spectroscopic Characterization of Charged Defects in Polycrystalline Pentacene by Time- and Wavelength-Resolved Electric Force Microscopy. *Adv. Mater.* **2011**, *23*, 624–628.
48. Pingree, L. S. C.; Reid, O. G.; Ginger, D. S. Electrical Scanning Probe Microscopy on Active Organic Electronic Devices. *Adv. Mater.* **2009**, *21*, 19–28.
49. Groves, C.; Reid, O. G.; Ginger, D. S. Heterogeneity in Polymer Solar Cells: Local Morphology and Performance in Organic Photovoltaics Studied with Scanning Probe Microscopy. *Acc. Chem. Res.* **2010**, *43*, 612–620.

50. Giridharagopal, R.; Ginger, D. S. Characterizing Morphology in Bulk Heterojunction Organic Photovoltaic Systems. *J. Phys. Chem. Lett.* **2010**, *1*, 1160–1169.
51. Li, J. B.; Chawla, V.; Clemens, B. M. Investigating the Role of Grain Boundaries in CzTs and CzTsSe Thin Film Solar Cells with Scanning Probe Microscopy. *Adv. Mater.* **2012**, *24*, 720–723.
52. Salvador, M.; Vorpahl, S. M.; Xin, H.; Williamson, W.; Shao, G. Z.; Karatay, D.; Hillhouse, H. W.; Ginger, D. S. Submitted.
53. Green, M. A.; Ho-Baillie, A.; Snaith, H. J. The Emergence of Perovskite Solar Cells. *Nat. Photonics* **2014**, *8*, 506–514.
54. Takihara, M.; Takahashi, T.; Ujihara, T. Minority Carrier Lifetime in Polycrystalline Silicon Solar Cells Studied by Photoassisted Kelvin Probe Force Microscopy. *Appl. Phys. Lett.* **2008**, *93*, 021902-1–021902-3.
55. Park, S. H.; Roy, A.; Beaupre, S.; Cho, S.; Coates, N.; Moon, J. S.; Moses, D.; Leclerc, M.; Lee, K.; Heeger, A. J. Bulk Heterojunction Solar Cells with Internal Quantum Efficiency Approaching 100%. *Nat. Photonics* **2009**, *3*, 297–302.
56. Moon, J. S.; Jo, J.; Heeger, A. J. Nanomorphology of PCDTBT: PC70BM Bulk Heterojunction Solar Cells. *Adv. Energy Mater.* **2012**, *2*, 304–308.
57. Cowan, S. R.; Roy, A.; Heeger, A. J. Recombination in Polymer-Fullerene Bulk Heterojunction Solar Cells. *Phys. Rev. B* **2010**, *82*, 245207.
58. Kronik, L.; Shapira, Y. Surface Photovoltage Phenomena: Theory, Experiment, and Applications. *Surf. Sci. Rep.* **1999**, *37*, 1–206.
59. Yakimov, A.; Forrest, S. R. High Photovoltage Multiple-Heterojunction Organic Solar Cells Incorporating Interfacial Metallic Nanoclusters. *Appl. Phys. Lett.* **2002**, *80*, 1667–1669.
60. Shikler, R.; Fried, N.; Meoded, T.; Rosenwaks, Y. Measuring Minority-Carrier Diffusion Length Using a Kelvin Probe Force Microscope. *Phys. Rev. B* **2000**, *61*, 11041–11046.
61. Foertig, A.; Kniepert, J.; Gluecker, M.; Brenner, T.; Dyakonov, V.; Neher, D.; Deibel, C. Nongeminate and Geminate Recombination in PTB7:PCBM Solar Cells. *Adv. Funct. Mater.* **2014**, *24*, 1306–1311.
62. Credgington, D.; Durrant, J. R. Insights from Transient Optoelectronic Analyses on the Open-Circuit Voltage of Organic Solar Cells. *J. Phys. Chem. Lett.* **2012**, *3*, 1465–1478.
63. Pasveer, W. F.; Cottaar, J.; Tanase, C.; Coehoorn, R.; Bobbert, P. A.; Blom, P. W. M.; de Leeuw, D. M.; Michels, M. A. J. Unified Description of Charge-Carrier Mobilities in Disordered Semiconducting Polymers. *Phys. Rev. Lett.* **2005**, *94*, 206601-1–206601-4.